15th Canadian Masonry Symposium
Ottawa, Canada
June 2-5, 2025

In-plane Cyclic Response of a Flexural Reinforced Masonry Core Wall with Boundary Elements

Amgad Mahrous[i], Belal AbdelRahman[ii], and Khaled Galal[iii]

ABSTRACT

Designing seismic-resistant mid- to high-rise reinforced masonry (RM) buildings requires an effective seismic force-resisting system (SFRS) that provides sufficient lateral strength and deformation capacity. Core walls are often chosen as the SFRS for reinforced concrete (RC) structures because they efficiently incorporate elevators, staircases, and utility shafts within the building core, maximizing floor space. These walls also offer flexibility in architectural layouts while maintaining structural integrity and seismic performance. Although much research has focused on RC core walls, little is known about the behavior of reinforced masonry core walls. This study experimentally evaluated the structural performance of a reinforced masonry core wall with boundary elements (RMCW+BEs) under lateral cyclic loading. The C-shaped RMCW+BEs was tested as a potential alternative to rectangular RM shear walls, offering improved structural and architectural benefits for typical RM buildings. The wall, representing the first story of a core wall in a 12-story building, demonstrated high ductility (14Δ_y) without losing lateral strength. The core wall exhibited a flexural-dominant ductile response, with a well-distributed crack pattern and significant energy dissipation. The findings suggest that RMCW+BEs could serve as an effective SFRS in RM buildings, contributing to the advancement of seismic-resistant construction and improving the resilience of RM buildings in North American seismic zones.

KEYWORDS

Core walls, Reinforced Masonry, Cyclic response, Quasi static, Lateral capacity, Ductility, Boundary Elements.

[i] PhD Graduate, Concordia University, Montreal, Canada, amgad.mahrous@mail.concordia.ca
[ii] Postdoctoral Fellow, Concordia University, Montreal, Canada, belal.abdelrahman@concordia.ca
[iii] Professor, Concordia University, Montreal, Canada, khaled.galal@concordia.ca

INTRODUCTION

With the advent of taller and more complex structures, the importance of reinforced concrete (RC) core walls has intensified. Their role in ensuring the structural integrity and resilience of high-rise buildings has become vital, driving ongoing research and innovation in core wall design, construction techniques, and material technologies.

On the other hand, reinforced masonry (RM) shear walls with boundary elements have become increasingly favoured as seismic force resisting system, SFRSs, particularly following the introduction of ductile RM shear walls in the 2015 National Building Code of Canada [1]. Additionally, the Canadian Standard for Design of Masonry Structures, CSA S304-14 [2], incorporated special seismic design and detailing guidelines for masonry boundary elements. The literature [3–9] has demonstrated through experimental and numerical investigations that reinforced masonry shear walls with boundary elements (RMSW+BEs) exhibit sufficient strength and ductility as SFRSs. Studies have indicated that including confined masonry boundary elements at the ends of walls markedly improves the ultimate strength and ductility capacity. The results suggest that the addition of boundary elements offers improved confinement for vertical steel bars, delaying reinforcement buckling and preventing crushing of the grout core in compression zones of the walls. Confined boundary elements contribute to enhancing the post peak behaviour of walls by preventing a strength reduction drop accompanied by cracking initiation and face shell spalling.

Hybrid structural systems combine different materials to take advantage of their respective strengths. For example, wood-structure tall buildings with a masonry core represent a sustainable approach to modern construction. On the other hand, combining fully grouted masonry shear/core walls with partially grouted gravity walls offers robust, yet economic solutions in tall buildings.

Although significant research has been dedicated to investigating the behaviour of RMSW+BEs and the widespread use of RC core walls, there is still a lack of experimental studies investigating the cyclic performance of reinforced masonry core walls with boundary elements (RMCW+BEs). Therefore, this study aims to assess the performance of RMCW+BEs under quasistatic cyclic loading along its major axis. The tested wall had an aspect ratio of 12.55 (12-story building) to replicate the seismic response of core walls utilized in mid-to-high-rise buildings. However, the first floor of the RMCW+BEs was physically tested in the laboratory, and the effect of the upper floors was simulated using the test protocol.

EXPERIMENTAL PROGRAM

The tested RMCW+BEs is one of the two C-shaped walls designed to resist the lateral load in a twelve-story residential building. The building is assumed to be located in a moderate seismic zone in North America (i.e., Montréal, Canada). The total height of the building is 36 m, with a typical story height of 3 m. The structural layout utilized in this study is composed of partially grouted RM walls designed to resist gravity loads and fully grouted RMCW+BEs as the main SFRS to resist the lateral load and some of the gravity loads. The building is designed following the guidelines of the NBCC 2020 [10], CSA S304-14 [2], TMS 402/602-22 [11] and NZS 4230 [12]. More details about the guidelines and design details for this structural layout can be found in a previous study by the authors [7]. Figure 1 shows the building plan. Precast flat slabs were assumed to distribute the gravity loads to the vertical structural elements. The core wall is composed of three ductile shear walls forming a C-shaped section. The RMCW+BEs had a web thickness of 190 mm, whereas the confined ends had dimensions of 390 × 390 mm. The partially grouted gravity walls have a rectangular cross-section with a thickness of 140 mm denoted as "G" on the layout, whereas the reinforced masonry core walls were denoted “C” on the layout. Figure 2 shows the cross-sectional details of the core and the gravity walls.

The core walls were designed to be RM ductile shear walls of the NBCC 2020 [10] and CSA S304-14, with a ductility-related force modification factor (R_d) of 3.0 and an overstrength-related force modification factor (R_o) of 1.5. The building was assumed to be built on clay soil with a soil classification of Class C following the NBCC 2020 guidelines.

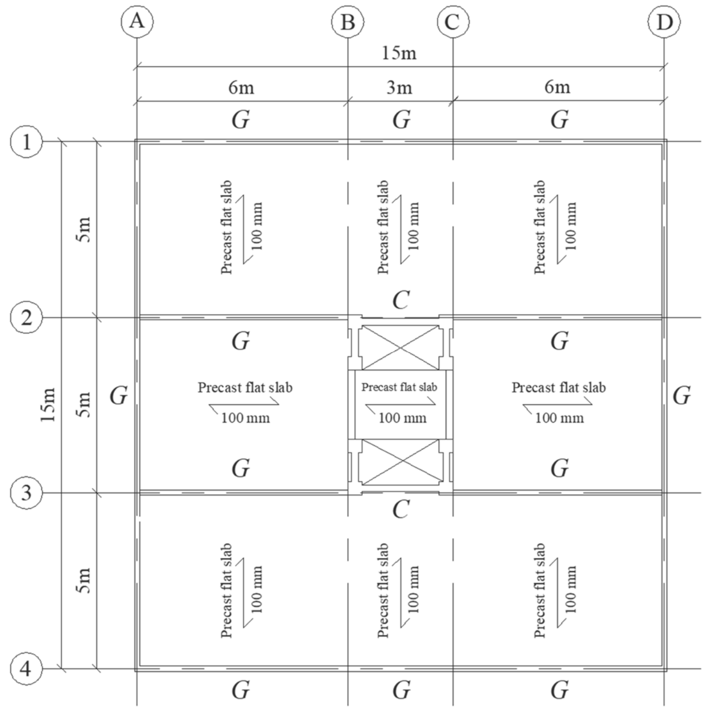

Figure 1. Structural layout

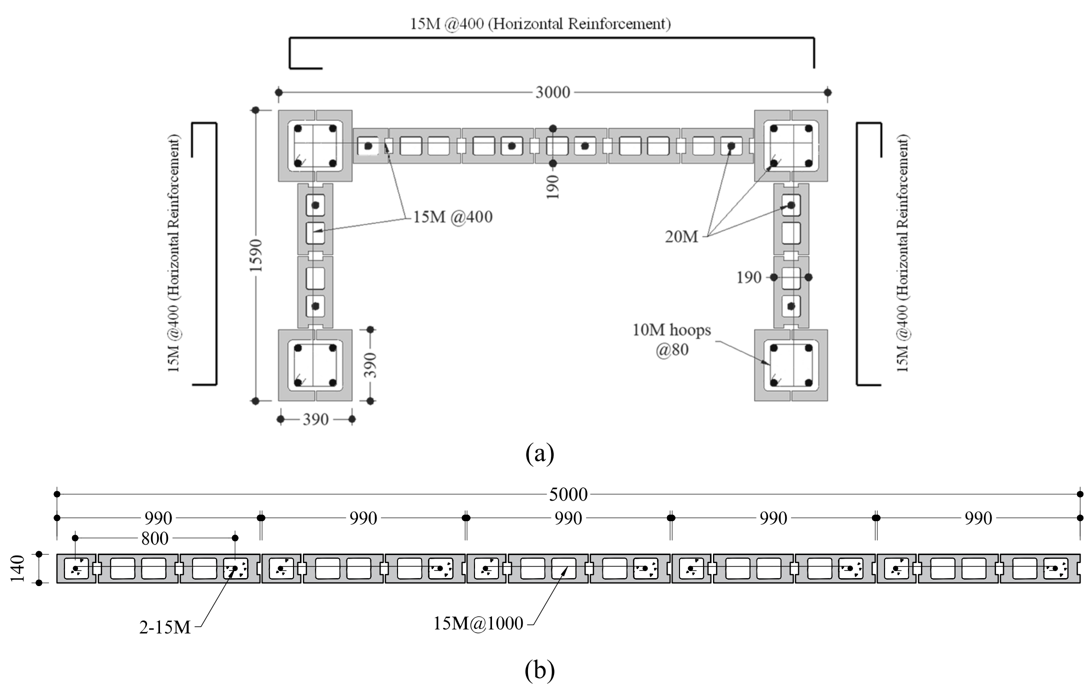

Figure 2. Typical details of RM walls: (a) Core; and (b) Gravity. (*dimensions in mm*)

One of the two core walls in the proposed prototype structure was selected to be tested in the east–west (E–W) direction under quasistatic cyclic loading. The selected direction represents the strong axis of the core wall. The core wall was then scaled to half of its scale to fit the test setup at Concordia University's Structures Lab. The first floor of the core wall was only constructed and tested under in-plane cyclic loading and a synchronized top moment to simulate the effect of the upper floors. The specimen was constructed using a half-scale stretcher and half-stretcher concrete masonry blocks for the web and flanges and C-shaped blocks for the boundary elements. The details of the reinforcement and dimensions of the scaled cross section are shown in Figure 3. The vertical reinforcement used for the boundary elements, web and flanges were #3 reinforcing bars that reflect the 20M reinforcing bars used in the full-scale specimen. The horizontal reinforcement was placed every other course with a standard 180° hook from one end and 90° from the other end, facilitating placement around the vertical reinforcing bars at the wall corners. The horizontal reinforcement consisted of D8 deformed wires, which represent the half-scale of the 15M reinforcing bars. Furthermore, the D4 deformed wires were used as seismic hoops with a 135° standard hook enclosing one of the vertical reinforcing bars at the boundary elements at a spacing of 40 mm. These wires represent the 10M reinforcing bars used in the full-scale prototype. A constant axial stress of 1.1 MPa was applied to the top of the wall, which represents a precompression ratio *($P/A_g\ f'_m$)* of 4.5%, where P is the axial load and A_g is the gross area of the wall's section. The design of the wall was intended to ensure flexure ductile failure, with its shear capacity surpassing the shear demand necessary for the formation of the plastic hinge mechanism at the base of the wall, adhering to the capacity design principle [13]. Additionally, the wall design ensured that the core wall possessed sufficient inelastic rotational capacity to satisfy the specifications outlined in CSA S304 [2] for the inelastic rotational demands of ductile walls.

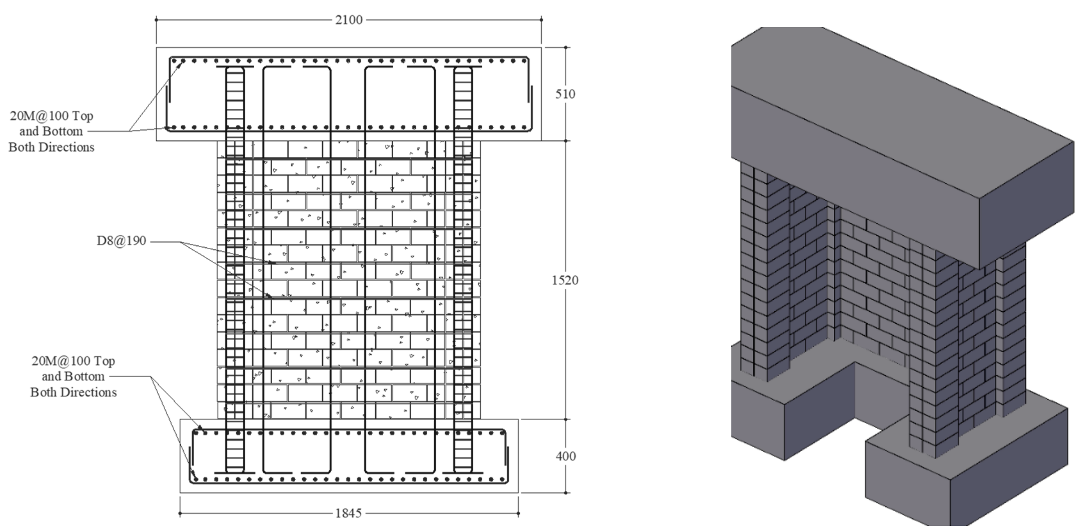

(a)

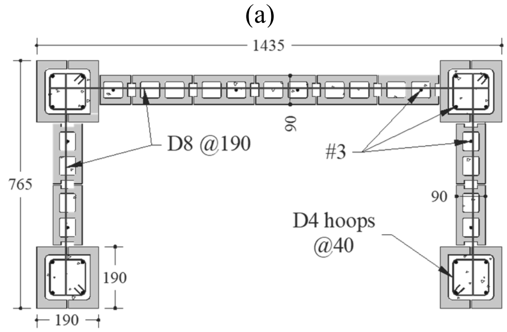

(b)

Figure 3. Specimen details: (a) Elevation and 3D view; and (b) Cross-section. ***(dimensions in mm)***

Concrete masonry blocks were tested from the same batch that was used in the wall construction, following the ASTM C140 [14] guidelines. Accordingly, six units from the stretcher blocks were tested and showed an average compressive strength of 38.5 MPa (CoV = 10.1%). On the other hand, the C-shaped blocks of the boundary elements were cut to shape a prismatic specimen with a height-to-thickness ratio of 2 and a length-to-thickness ratio of 4 with the final dimension of 100 × 50 × 25 mm, according to ASTM C140 guidelines. The prismatic specimens showed an average compressive strength of 23.2 MPa (CoV = 14.1%), based on a net cross section area of 100 × 25 = 2500 mm^2. The 50-mm mortar cube specimens were sampled and tested in accordance with the CSA A179 [15] and ASTM C109 [16] standards. The average compressive strength of the mortar was 23.3 MPa (COV = 16.7%). The web, flanges, and boundary element areas of the wall were filled with ordinary strength fine grout. The average compressive strength of the grout cylinders was 21 MPa, which was tested in accordance with CSA A179.

Masonry prisms of the web and flanges were one block in length and four blocks in height (190 × 380 mm), while the boundary element prisms were constructed using four courses of C-shaped blocks to match the dimensions of the square boundary elements (190 × 190 mm). The prisms were grouted using the same batch used for grouting the wall. Three prisms representing the flange/web and three boundary element prisms were tested in accordance with ASTM C1314 [17] to assess the specified compressive strength (f_m'). The results showed average compressive strengths of 24.2 MPa (CoV = 6.3%) and 16.5 MPa (CoV = 9.2%) for the flange/web prisms and boundary element prisms, respectively. Five specimens of each reinforcing bar and wire size were tested under axial tension according to ASTM A370 [18]. The #3 reinforcing bars showed an average yield strength (f_y) of 455 MPa (CoV = 1.6%), an average yield strain (ε_y) of 0.00227 mm/mm, and an ultimate strength (f_u) of 689 MPa (CoV = 2.6%) with an ultimate strain (ε_u) of 0.0941 mm/mm. The D4 and D8 deformed wires showed average yield strengths (f_y) of 600 MPa and 536 MPa (CoV = 5.6%), respectively, based on the 0.2% strain offset method in ASTM A1064 [19], in instances where there is no well-defined yield point. In contrast, the D4 wires exhibited an average ultimate strength (f_u) of 658 MPa (CoV = 10.8%) with an average ultimate strain (ε_u) of 0.0212 mm/mm. The D8 wires showed an average ultimate strength (f_u) of 585 MPa (CoV = 0.9%) with an average ultimate strain (ε_u) of 0.0304 mm/mm.

TEST SETUP

The tested wall is the half-scale version of one of the core walls used as the main SFRS of the 12-story RM prototype building. However, the wall physically constructed in the laboratory represents the 1st floor of the 12-story core wall. The wall shear span-to-depth ratio (M/Vd) was 10.4. The shear span-to-depth ratio was calculated by dividing the effective height (h_{eff}) by the depth of wall (d). The effective height was taken as two-third of the 12-story wall's height based on the assumed triangular lateral load distribution, while the depth was estimated as 0.8 of the total length of the wall (l_w) of the web length. The wall was tested by applying lateral displacement at the top, in addition to the top overturning moments. The lateral displacements applied with the horizontal actuator were synchronized with the applied top moments using the two vertical actuators. Figure 4 shows the details of the test setup. Lateral displacements were applied to the top of the wall by means of an RC loading beam using a displacement-controlled actuator with a capacity of ± 734 kN and a maximum stroke of ± 200 mm. Furthermore, the axial compression load and the top moments were applied using two vertical force-controlled actuators with the same capacity and stroke as the horizontal actuator. The bottom footing of the wall was connected to a larger transfer RC footing using eighteen 25.4 mm (1 in.) high-strength prestressing rods. This arrangement ensured a fixed boundary condition at the base of the wall. The transfer RC footing, in turn, was secured to the laboratory's strong floor using twelve 50.8 mm (2 in.) high-strength prestressing bolts.

A constant axial load of 318 kN, equivalent to an axial stress of 1.1 MPa based on the design of the prototype building, was applied to the wall using two vertical actuators during the loading history of the wall. Then, the horizontal actuator was used to apply a lateral displacement until it reached the target displacement of each cycle. For each target displacement, the force in the horizontal actuator is used to calculate the coupling forces (i.e., top moment) that need to be applied by the two vertical actuators. The top moment is calculated by assuming an inverted triangle lateral-load shape along the wall height. The displacement-control loading protocol followed ASTM E2126 [20]. The first yield of the outermost vertical reinforcing bars at the footing-wall interface was selected as the representative damage state of the wall. The installed strain gauges on the vertical reinforcement at the wall-foundation interface were used to obtain the yield strain (ε_y). The displacement that corresponds to the first yield strain of the outermost reinforcing bars is defined as the yield displacement (Δ_y), which was obtained by displacing the wall in reversible cycles with displacement increments equal to 25%, 50%, 75%, and 100% of the yield strain of the vertical reinforcing bars. The yield displacement was then calculated as the average displacement for the push and pull directions at which the outermost vertical reinforcing bars reached the yield strain. Subsequently, the wall was subjected to reversible cycles with a target displacement equal to multiples of its yield displacement ($2\Delta_y$, $3\Delta_y$, $4\Delta_y$, $5\Delta_y$,...). The wall was tested until it reached a 20% capacity degradation.

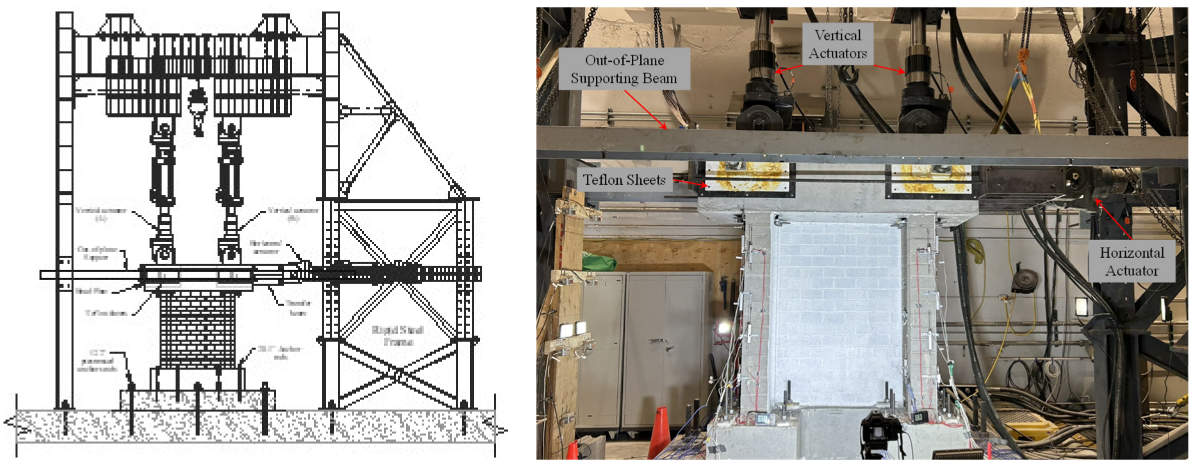

Figure 4. Details of the test setup.

Results and Discussion

Figure 5 shows the load–displacement hystereses of the wall. The top drift of the wall was obtained by dividing the lateral displacements measured at the wall's top by the height of the specimen. The average lateral displacement for the push and pull directions of the wall was 3.21 mm at the onset of the first yield (Δ_y), corresponding to a drift ratio of 0.21% and a lateral force at yield (Q_y) of 50.42 kN. There was a slight difference in the yield displacement between the two loading directions of 12.5%. However, the force corresponding to the onset of yield had a negligible difference of 2.4%. The wall showed an average peak load (Q_u) at $14\Delta_y$ of 66.80 kN with a corresponding lateral displacement (Δ_{Qu}) of 43.27 mm and a drift ratio of 2.82%. The wall sustained a maximum lateral displacement level of $17\Delta_y$ at a 20% capacity degradation, where the ultimate load recorded for the wall ($Q_{0.8u}$) was 52.45 kN with a corresponding lateral displacement ($\Delta_{0.8Qu}$) of 52.5 mm and an equivalent drift ratio of 3.43%.

The wall showed a stable ductile load–displacement response without any significant reduction in the lateral capacity until reaching $15\Delta_y$. The hysteretic behavior of the wall showed an almost symmetrical response for the push and pull directions, which reflected the uniformity of the wall cross section. Furthermore, the wall was able to withstand substantial inelastic deformations beyond the measured displacement at yield without experiencing substantial degradation in lateral capacity.

The core wall showed significant horizontal cracks accompanied by the yielding of the vertical reinforcement of the outermost reinforcing bars and crushing of the masonry boundary elements at the compression zones of the wall-foundation interfaces. This reflects the dominance of the flexure response on the wall's behavior. Figure 6 shows that at the onset of the first yield displacement, the specimen exhibited minimal horizontal flexural cracks passing through the mortar bed joints on all the faces of the wall. The horizontal cracks started to propagate horizontally, forming stepped cracks at the mortar vertical joints in the subsequent cycles.

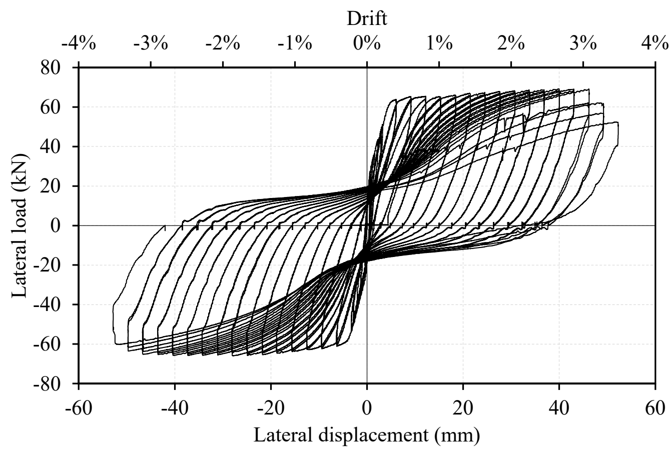

Figure 5. Load–displacement Hysteresis Loops

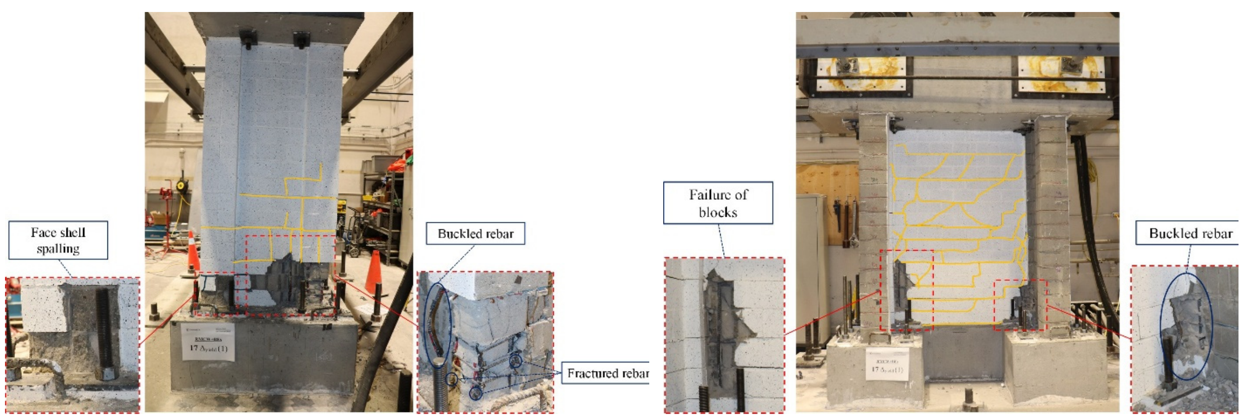

(a) (b)

Figure 6. Damage states of the tested core wall: (a) Wall north view; and (b) Wall east view.

Curvature Ductility

The vertical deformations obtained using the five LVDTs attached to the four boundary elements of the wall, which were utilized to estimate the average vertical compressive (ε_m) and tensile (ε_s) strains. The LVDTs are equally spaced over the wall's height with an identical gauge length of almost 304 mm. The average curvature (φ_i) was calculated for each of the five segments of the wall as the ratio between the summation of the compressive and tensile strain.

Figure 7 presents the obtained average curvature profiles for 1, 3, 6, 9, 12, and 15Δ_y along the wall height for the push and pull directions. Notably, the presented curvature profiles are based on the compressive and tensile strains calculated from the vertical deformations of the LVDTs attached to the northern boundary elements of the east and west flanges. This is based on the effects of the shear lag that resulted in maximum strains at those two referred locations. Shear lag influences the stress distribution and design capacity of nonplanar shear walls with flanges (i.e., C-shaped, L-shaped, or T-shaped). The non-uniform stress distribution due to shear lag effects across the flange width leads to potential reductions in the effective stiffness and strength of the wall system. The curvature profile is obtained up to the 1st cycle of 15Δ_y before losing the bottom LVDT, L2, due to face shell spalling. The wall showed an average yield curvature (φ_{iy}) of 2.6×10^{-6} rad/mm. The average curvature at peak load was obtained at 15$\Delta_{y,}$ with an average value of 3.5×10^{-5} rad/mm. The maximum curvature was almost 13 times the yield curvature. This value is also defined as the curvature ductility (μ_φ), which is calculated as the ratio between the ultimate curvature (φ_{iu}) and the curvature at yield (φ_{iy}).

The vertical strains in relation to the normalized wall length are depicted in Figure 8. The vertical deformations of LVDTs L2, L23, L24, and L8 were used to calculate the strain profile over a gage length of 304 mm. The strain profiles are displayed for both loading directions at designated ductility levels (i.e., 1, 3, 6, 9, 12, and 15Δ_y). Positive values represent compressive axial strain, and tensile strains are represented by negative values. At low ductility levels (3Δ_y), it is evident that the strain profiles were relatively linear and exhibited a near-symmetric behavior in both the push and pull loading directions. As the ductility demands increased, broken lines started to become apparent toward the boundary element edges. However, a large number of instruments need to be mounted on the wall surface at different locations to obtain an accurate strain profile, especially at boundary element-web interfaces.

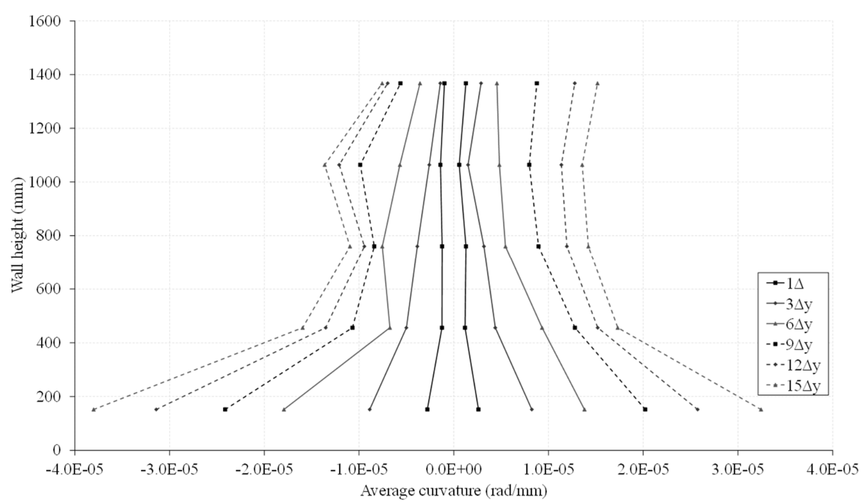

Figure 7. Curvature along the wall height.

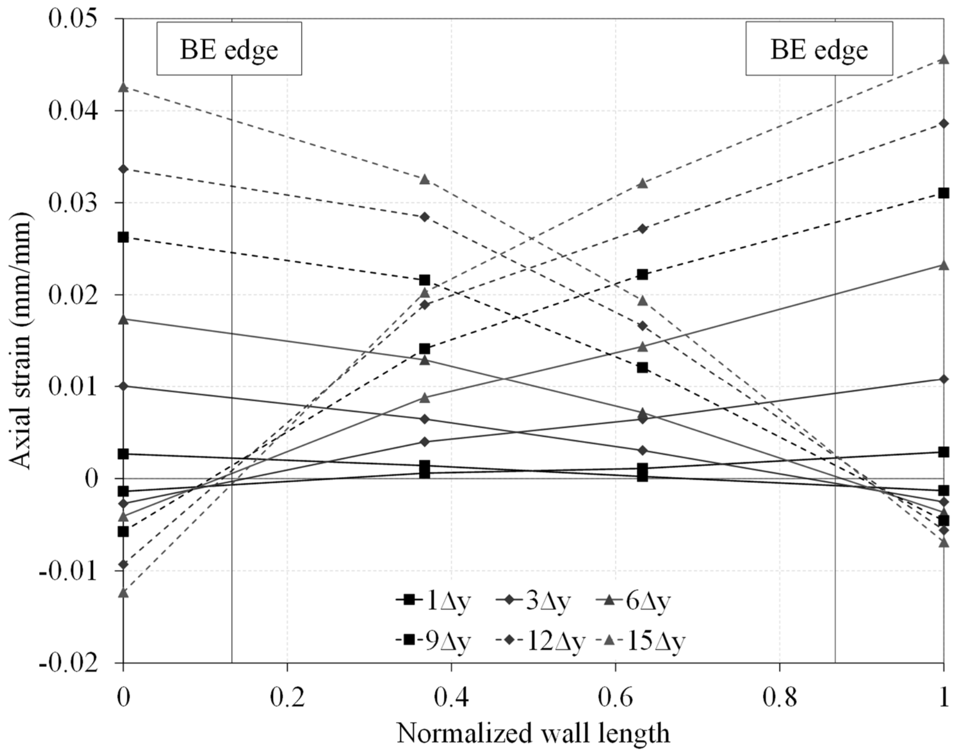

Figure 8. Strain profile along the wall length.

Displacement Ductility

The displacement ductility at the peak load (μ_{Qu}) was determined by dividing the lateral displacement corresponding to the peak load (Δ_{Qu}) by the lateral displacement recorded at the first yield (Δ_y) of the outermost vertical reinforcing bars. Similarly, the ultimate displacement ductility ($\mu_{0.8Qu}$) was obtained by dividing the lateral displacement corresponding to a 20% load reduction ($\Delta_{0.8Qu}$) by the lateral displacement at the first yield (Δ_y). The wall showed high values of displacement ductility, where the displacement ductility at peak load (μ_{Qu}) was 14.4, and the ultimate displacement ductility ($\mu_{0.8Qu}$) was 17.5.

Stiffness Degradation

Figure 8 depicts the relationships between the ratios of the secant stiffness (K_e) to the initial stiffness (K_i) and the secant stiffness (K_e) to the yield stiffness (K_y) of the tested wall with respect to different displacement ductility levels. The initial stiffness (K_i) is determined as the ratio between the lateral displacement and the lateral resistance at $0.25\Delta_y$. The secant stiffness (K_e) is calculated as the slope of the line connecting the maximum and minimum peak points of the hysteresis loop. The yield stiffness is calculated using the same method but considering the values at $1\Delta_y$. The calculated secant stiffness at the onset of yielding decreased to around 30% of the initial stiffness of the wall. In other words, the secant stiffness at $0.25\Delta_y$ was 3.2 times the secant stiffness at yield. The wall showed a drop in the initial stiffness of 81% at the end of the test (i.e., $17\Delta_y$). The significant reduction in the wall stiffness during the initial loading cycles indicates an increase in the natural period of vibration with a decrease in the lateral capacity. This can be attributed to the enhanced detailing of the boundary elements that led to an improvement in structural performance and ductility. However, as the lateral displacements increase further, there is a slight degradation in the wall's stiffness, demonstrating a reduced elongation during the natural period.

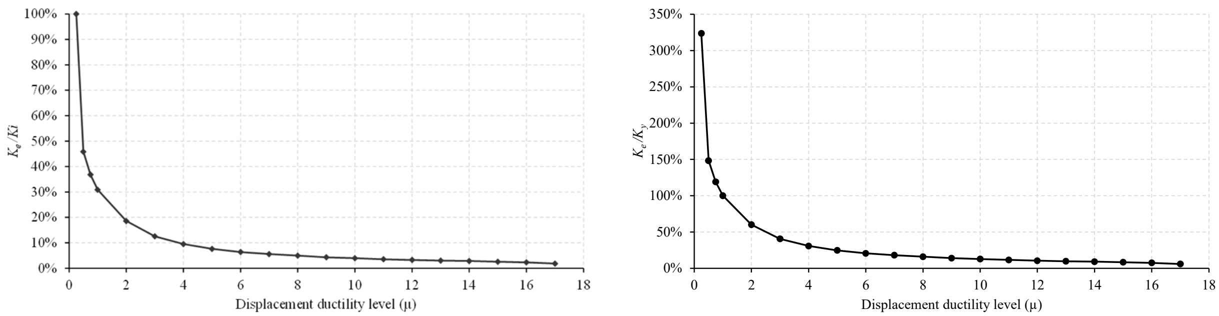

(a) (b)

Figure 8. Effect of ductility on stiffness degradation: (a) Effective stiffness to secant stiffness ratio; and (b) Effective stiffness to yield stiffness ratio.

CONCLUSION

This study investigated the structural flexural behavior of a reinforced masonry core wall with boundary elements (RMCW+BEs) subjected to unidirectional in-plane lateral cyclic loading along its major axis. The wall represents the first story of typical walls utilized as the main SFRS in a 12-story prototype building. The effect of the upper stories was simulated by synchronized top moments using two vertical actuators attached to the wall's top. The hysteresis loops observed for the tested wall exhibited symmetrical responses in both loading directions. Initially, thin loops implied nearly elastic responses during the early stages of loading, while larger loops indicated greater energy dissipation associated with inelastic responses at higher displacement levels. The wall showed a stable ductile load–displacement response without any significant reduction in the lateral capacity until reaching $15\Delta_y$. In addition, the wall showed a considerably high drift level at the maximum load of 2.82% without any reduction in its lateral capacity. The wall damage sequence was characterized by a dominant flexural response, where horizontal cracks accompanied by the yielding of the vertical reinforcement of the outermost reinforcing bars occurred. The wall attained a high ductility level of $14\Delta_y$ without experiencing a degradation in the wall's lateral capacity and an acceptable damage level. This study highlights the behaviour of RMCW+BEs as a potential seismic force-resisting system.

ACKNOWLEDGEMENTS

The authors acknowledge the financial support of the Natural Sciences and Engineering Research Council of Canada (NSERC), Canadian Concrete Masonry Producers Association (CCMPA), Canada Masonry Design Center (CMDC), and Fonds de Recherche du Québec – Nature et Technologies (FRQNT).

REFERENCES

[1] NBCC. National Building Code of Canada, National research council of Canada. Ottawa: NBCC 2015.

[2] CSA. Design of Masonry Structures. CSA S304. Rexdale, ON, Canada: CSA: 2014.

[3] Shedid MT, El-Dakhakhni WW, Drysdale RG. Characteristics of Rectangular, Flanged, and End-Confined Reinforced Concrete Masonry Shear Walls for Seismic Design. J Struct Eng 2010;136:1471–82.

[4] Heerema P, Shedid M, El-Dakhakhni W. Seismic Response Analysis of a Reinforced Concrete Block Shear Wall Asymmetric Building. J Struct Eng 2015;141. https://doi.org/10.1061/(ASCE)ST.1943-541X.0001140.

[5] Ezzeldin M, El-Dakhakhni W, Wiebe L. Reinforced Masonry Building Seismic Response Models for ASCE/SEI-41. J Struct Eng 2018;144:1–13.

[6] Obaidat AT, Ashour A, Galal K. Stress-Strain Behavior of C-Shaped Confined Concrete Masonry Boundary Elements of Reinforced Masonry Shear Walls. J Struct Eng 2018;144:04018119.
[7] Mahrous A, AbdelRahman B, Galal K. Seismic response analysis of reinforced masonry core walls with boundary elements. Eng Struct 2022;270:114882.
[8] Aly N, Galal K. Effect of Ductile Shear Wall Ratio and Cross-Section Configuration on Seismic Behavior of Reinforced Concrete Masonry Shear Wall Buildings. J Struct Eng 2020;146:1–15.
[9] AbdelRahman B, Galal K. Sensitivity of the seismic response of reinforced concrete masonry walls with boundary elements to design parameters. Eng Struct 2022;255:113953. https://doi.org/10.1016/j.engstruct.2022.113953.
[10] NBCC. National Building Code of Canada: 2020 2022. https://doi.org/10.4224/w324-hv93.
[11] TMS. "The Masonry Society" 402/602-22 Building Code Requirements and Specification for Masonry Structures. Masonry Society; 2022.
[12] New Zealand Standard. Design of reinforced concrete masonry structures. NZS 4230. Wellington, New Zealand: NZS: 2004.
[13] Paulay, T . and Priestley MJN. Seismic design of reinforced concrete and masonry buildings. 1992.
[14] ASTM. Standard Test Methods for Sampling and Testing Concrete Masonry Units and Related Units. Am Soc Test Mater 2022;15:21–6. https://doi.org/10.1520/C0140.
[15] CSA-A179. National Standard of Canada CAN / CSA-A179-14 Mortar and grout for unit masonry 2014;14.
[16] ASTM C109. Standard test method for compressive strength of hydraulic cement mortars. Am Soc Test Mater 2022;04:1–7. https://doi.org/10.1520/C0109.
[17] ASTM C1314. Standard Test Method for Compressive Strength of Masonry Prisms. Am Soc Test Mater 2021:1–10. https://doi.org/10.1520/C1314-18.2.
[18] ASTM A370 A. Standard Test Methods and Definitions for Mechanical Testing of Steel Products. Am Soc Test Mater 2022;14:4–5. https://doi.org/10.1520/A0370-22.2.
[19] ASTM A1064. Standard Specification for Steel Welded Wire Reinforcement , Plain , for Concrete. Am Soc Test Mater 2018:1–6. https://doi.org/10.1520/A1064.
[20] ASTM E2126 A. Standard Test Methods for Cyclic (Reversed) Load Test for Shear Resistance of Vertical Elements of the Lateral Force Resisting Systems for Buildings. ASTM E2126. 2019. https://doi.org/10.1520/E2126-19.